Subramanian and Cherukuri *Integrating Materials and Manufacturing Innovation* 2014, **3**:27
http://www.immijournal.com/content/3/1/27

Integrating Materials and Manufacturing Innovation
a SpringerOpen Journal

RESEARCH Open Access

Prediction of microstructure evolution during multi-stand shape rolling of nickel-base superalloys

Kannan Subramanian[1*] and Harish P Cherukuri[2]

*Correspondence:
ksubramanian@stress.com
[1]Stress Engineering Services, Inc., 3314 Richland Ave, 70002 Metairie, LA, USA
Full list of author information is available at the end of the article

Abstract

In this paper, a comprehensive numerical approach to predict the microstructure of nickel-base superalloys during multi-stand shape rolling is presented. This approach takes into account the severe deformation that occurs during each pass and also the possible reheating between passes. In predicting the grain size at the end of the rolling process, microstructural events such as dynamic recrystallization (DRX), metadynamic recrystallization (MDRX), and static grain growth are captured at every deformation step for superalloys. Empirical relationships between the average grain size from various microstructural processes and the macroscopic variables such as temperature (T) and effective strain ($\bar{\varepsilon}$) and strain rate ($\dot{\bar{\varepsilon}}$) form the basis for the current work. These empirical relationships are based on Avrami equations. The macroscopic variables are calculated using a finite element analysis package wherein the material being rolled is modeled as a non-Newtonian fluid with viscosity that depends on the effective strain rate, strain, and temperature. A two-dimensional transient thermal analysis is carried out between passes that can capture the MDRX and/or static grain growth during the microstructural evolution. The presented microstructure prediction algorithm continuously updates two families of grains, namely, the recrystallized family and strained family at the start of deformation in any given pass. In addition, the algorithm calculates various subgroups within these two families at every deformation step within a pass. As the material undergoes deformation between the rolls, recrystallization equations are invoked depending on critical strain and strain rate conditions that are characteristics of superalloys. This approach predicts the microstructural evolution based on recrystallization kinetics and static grain growth only. The methodology was successfully applied to predict the microstructure evolution during the multi-pass rolling of nickel-base superalloys. The predicted results for Alloy 718 for a 4-stand rolling followed by air cooling and for a 16-stand rolling followed by a combination of air and water cooling are also compared with experimental observations.

Keywords: Multi-stand; Multi-pass; Shape rolling; Microstructure; Modeling; Nickel-base; Superalloys

Background

Superalloys are used for high temperature (>650°C) applications such as those encountered in the aircraft, petrochemical, and nuclear utility industries and where resistance to deformation is a primary requirement. Nickel-base alloys such as Waspaloy and Alloy 718 (IN 718) are examples of superalloys that resist deformation at elevated temperatures and are therefore difficult to hot work. Hot working is the term often used to describe the plastic deformation at temperatures high enough to overcome strain hardening. The major hot-working operations are open-die press forging, radial forging, extrusion, and rolling. In the case of rolling and forging, there may be many passes and some reheats involved. In this paper, the hot-working operation under consideration is the continuous shape rolling process. In the considered shape rolling process, billets transform from round-to-oval and oval-to-round until the desired shape and size are obtained in multiple stands or passes.

At a given alloy composition, the high temperature flow stress is largely influenced by the grain size of the microstructure. During shape rolling, the correct working forces, which relate to gauge and shape control as well as to power requirements, can be estimated accurately only if the microstructure relevant to the specific pass of rolling is known. The microstructure present at the end of the rolling and cooling operations also controls the product properties. Coarser grain size (ASTM 4 to 8) favors creep strength and crack-growth resistance while a fine grain (ASTM 10 to 14) structure favors improved low-cycle fatigue life and tensile yield strength. In addition, control of grain size is an important characteristic in any hot-working due to the stringent ultrasonic inspectability requirements.

Modeling the microstructural changes due to deformation during a multi-pass continuous rolling is the main focus of this paper. Due to the severe economical and practical aspects of industrial trials and laboratory experiments, numerical methods are often used to study the influence of the vast number of variables present in a typical industrial multi-stand rolling on the mictrostructure. Currently, numerical techniques based on the finite element (FE) method are extensively used in solving plastic deformation problems. Process variables such as strain and temperature are predicted from FE analysis of the deformation process. In general, microstructural modeling relates those process variables to microstructural evolution. Typical microstructural modeling involves two major steps. In the first step, constitutive equations describing the microstructural evolutions are developed using experiments. In the second step, the microstructural constitutive equations are implemented in commercial FE packages or a custom-built software.

In this paper, a comprehensive microstructure prediction methodology specifically suited for nickel-base superalloys is presented and validated in the context of multi-stand rolling involving flow formulation. Information on microstructure prediction can be found in the open literature for non-superalloy materials such as steel and aluminum that do not have a clear distinction between some of the microstructural events found in superalloys. In addition, microstructure prediction techniques do not appear to be currently available for multi-stand shape rolling of nickel-base superalloys where the number of stands may be as high as 16. This is attributed to the fact that conducting experiments and gathering data for multi-stand rolling result in significant down-time of the equipment. Furthermore, numerical simulations to model multi-stand rolling are also expensive to carry out due to the large deformations, contact conditions, and

thermomechanical couplings involved. Therefore, this paper focuses primarily on a flow-formulation based on the primary goal of predicting microstructure expeditiously so that real-time control of multi-stand rolling can be achieved. The approach is validated using experimental data for four stands [1] and then for 16 stands [2]. In contrast, a vast majority of current FE methods simulate shape rolling using rigid plastic or elastoplastic formulations with microstructure as internal variables which is computationally intensive and real-time predictions are not feasible.

This paper is organized as follows. In the 'Methods' section, a discussion of the finite element formulation of the multi-stand shape rolling process is provided. An introduction to the microstructural processes, models, and microstructure evolution algorithm is also discussed in the 'Methods' section. Alloy 718, the alloy for which results are presented in this work, is governed by the fcc lattice structure of the γ matrix [3] and a number of characteristic precipitates such as γ'' (Ni3(Nb,Ti)), γ', δ, and carbides (MC and M6C). The high temperature strength of Alloy 718 is derived essentially from the coherent γ'' and to a smaller extent from γ'. The presence of the other precipitates improves hot-working to produce very fine-grained billet structures. However, modeling the complex precipitation processes requires a more detailed understanding of precipitation kinetics than is presently available. A mechanism-based model considering the δ phase precipitate effects has been discussed in literature by Thomas, et al. [4]. The proposed phenomenological model in this work results in good agreement with the observed microstructure as long as it is applied to materials where the initial microstructure does not contain excessive δ phase since these precipitates retard metadynamic recrystallization (MDRX). The proposed model is recommended when the rolling occurs at temperatures above δ solvus as observed in this work. Due to this, the current work aims to find the average grain sizes from recrystallization processes alone and does not take into account the precipitation of phases. The results are discussed and conclusions and future direction are provided in the last two sections of this paper.

Methods

Since the microstructure prediction methodology is closely tied to the FE formulation of the continuous shape rolling process, a brief discussion of the FE approach is presented initially. This is followed by a discussion on the microstructure prediction methodology.

FE formulation of multi-stand rolling

The multi-stand shape rolling process is simulated using an FE code in which the material behavior is modeled as that of a non-Newtonian fluid with a viscosity that is dependent on the temperature, strain rate, and effective strain. In this flow formulation, the governing momentum and energy balance equations are solved simultaneously to find the steady-state velocity components and the temperature at each node while satisfying the incompressibility constraint. A transient heat transfer analysis is carried out between the passes to take into account the heating or cooling between the passes.

The three-dimensional FE mesh corresponding to the control volume considered in the analysis consists of a number of equi-sized slices. Initially, a two-dimensional mesh using quadrilaterals (see Figure 1a) is generated. With appropriate connectivity between the nodes of cross-sectional elements in any given slice, the three-dimensional mesh is created (see Figure 1b). The three-dimensional element considered for the analysis is

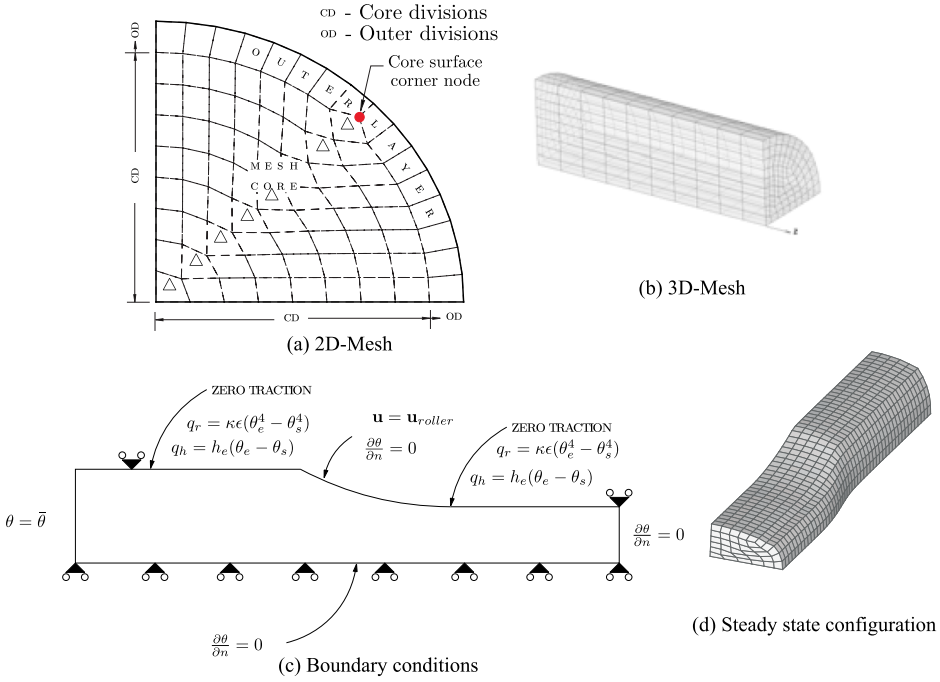

Figure 1 FE mesh (a, b), BCs (c), and steady-state configuration (d).

the commonly used brick element (tri-linear hexahedron) with *velocity-pressure* (*u-p*) formulation capabilities.

A brief description of the flow formulation is given in the following. The augmented potential energy functional for the flow under consideration is

$$J^* = \int_\Omega \sigma'_{ij}\dot{\varepsilon}_{ij}d\Omega - \int_{\Gamma_t} \bar{T}_i u_i d\Gamma + \int_\Omega p\dot{\varepsilon}_{ii}d\Omega. \tag{1}$$

In the absence of body forces, the first and second terms in Equation 1 represent the rates of internal and external works, respectively, while the last term represents the addition of incompressibility constraint in the flow potential. Upon substituting the constitutive equation, $\sigma'_{ij} = 2\mu\dot{\varepsilon}_{ij}$, and applying Gauss theorem, the first variation of this functional simplifies to

$$\delta J^* = \int_\Omega \dot{\varepsilon}_{ij} 2\mu\delta\dot{\varepsilon}_{ij}d\Omega - \int_{\Gamma_t} \bar{T}_i\delta u_i d\Gamma + \int_\Omega p\delta\dot{\varepsilon}_{ii}d\Omega + \int_\Omega \delta p\dot{\varepsilon}_{ii}d\Omega. \tag{2}$$

If $\mathbf{K}_D$ and $\mathbf{Q}$ refer to the stiffness contribution for velocity and pressure, respectively, the FE formulation of Equation 2 leads to

$$\begin{bmatrix} \mathbf{K}_D & \mathbf{Q} \\ \mathbf{Q}^T & \mathbf{0} \end{bmatrix} \begin{Bmatrix} \mathbf{u} \\ \mathbf{p} \end{Bmatrix} = \begin{Bmatrix} \mathbf{f} \\ \mathbf{0} \end{Bmatrix}.$$

The above system is augmented with a penalty function [5], typically the Lagrange multiplier γ:

$$\begin{bmatrix} \mathbf{K}_D & \mathbf{Q} \\ \mathbf{Q}^T & -\frac{1}{\gamma}\mathbf{I} \end{bmatrix} \begin{Bmatrix} \mathbf{u} \\ \mathbf{p} \end{Bmatrix} = \begin{Bmatrix} \mathbf{f} \\ -\frac{1}{\gamma}\mathbf{p} \end{Bmatrix}.$$

This can be iteratively solved to determine the pressure and velocity as follows:

$$\mathbf{p}^{i+1} = \mathbf{p}^{i} + \gamma\left(\mathbf{Q}^{T}\mathbf{u}^{i}\right)$$
$$\left[\mathbf{K}_{D} + \gamma\left(\mathbf{Q}\mathbf{Q}^{T}\right)\right]\mathbf{u}^{i+1} = \mathbf{f} - \mathbf{Q}\mathbf{p}^{i+1}.$$

In a similar manner, a finite element formulation using Galerkin's weighted residual method is applied for the coupled heat transfer equations. Appropriate boundary conditions (see Figure 1c) are applied and the steady-state configuration (see Figure 1d) is determined. In this shape rolling approach, the locations of the nodes at the steady state are obtained by an iterative method using a modified Euler integration of the current velocity field. This FE formulation was (previously) successfully implemented for a four-stand multi-stand rolling [1]. In the present work, this FE formulation is adopted to analyze 16 or more stands [2].

Microstructure evolution and algorithm

Microstructure theory

Work hardening and dynamic softening coexist during hot deformation of nickel-base superalloys. Various deformation parameters such as strain, strain rate, and temperature influence the microstructure. The strain rate accelerates the accumulation of dislocations that results in strain-rate hardening. Temperature is related to the softening process through the resulting decrease or rearrangement of dislocations. In general, the thermomechanical processing encompasses recovery, recrystallization, and grain growth. Recovery and/or recrystallization may occur during deformation at high temperatures which are the common softening or restoration processes. In addition, the rates of cooling of the material are generally very low in large-scale metal forming operations, allowing recovery, recrystallization, and grain growth to occur immediately after hot deformation. These dynamic restoration processes are different from the static annealing processes which occur during post-deformation heat treatment. These processes are of special importance to the metal industry as they lower the flow stress of the material and enable the material to deform more easily. In addition, they also have an influence on the texture and the grain size of the worked material. In the case of metals of low or medium stacking fault energy (copper, nickel, and austenitic iron), the recovery processes are slow, and dynamic recrystallization dominates after a critical deformation condition is reached [6].

Microstructure evolution

During high strain and strain-rate thermomechanical processes such as multi-stand rolling, recrystallization is the major restoration process followed by static grain growth between passes that influences the development of microstructure. Therefore, further discussion will focus only on the details of recrystallization and grain growth listed below:

- Dynamic recrystallization (DRX)
- Metadynamic recrystallization (MDRX)
- Static grain growth (SGG)

DRX occurs during deformation when the strain exceeds a certain critical strain $\bar{\varepsilon}_c$. Use of critical strain can be found in a pioneering work by Sellars [7]. This occurs somewhat before the peak of the stress-strain curve. In this process, the nuclei for recrystallization are formed. MDRX occurs after deformation because the strains required to complete the

DRX are not continuously achieved. The strains are still greater than the critical strain $\bar{\varepsilon}_c$. During MDRX no new nuclei are formed but the dislocation density is reduced. Even though the straining is stopped, annealing continues and the existing nuclei will grow.

The progress of recrystallization during isothermal annealing is commonly represented by the volume fraction of material recrystallized (X) using a sigmoidal curve given as follows,

$$X = 1 - \exp\left(-\beta x^n\right). \tag{3}$$

In Equation 3, x can be time or strain, depending on the phase of recrystallization process discussed later. This is commonly known as the Johnson-Mehl-Avrami-Kolmogorov (JMAK) model. β is typically a function of the rate at which the nuclei are formed and the rate at which the grains grow. The exponent n is usually defined as JMAK or Avrami exponent. A significant feature of the JMAK approach is that the nucleation sites are assumed to be randomly distributed. However, it is too simple to quantitatively model a process as complex as recrystallization. The strain rate and deformation temperature are often incorporated into a single parameter, the 'Zener-Hollomon parameter' (Z) also known as the 'temperature compensated strain rate', defined as:

$$Z = \dot{\varepsilon} \exp\left(\frac{Q}{RT}\right), \tag{4}$$

where Q is the activation energy of the process. In the present work, the flow stress is incorporated in the FE formulation as a function of temperature, strain, and strain rate in a tabular form.

When the material is fully recrystallized, further grain growth may occur. Static grain growth occurs after deformation. The strains are less than the critical strain $\bar{\varepsilon}_c$.

Empirical modeling

Empirical laws describing the various processes mentioned above establish the relationships between grain size and process parameters such as tool and workpiece geometry, temperature, deformation speed, and amount of deformation through regression analysis of experimental data as developed by Huang et al. [8] and Shen [9]. Sellars [7] considered the relationship between the grain size obtained after each process (DRX and MDRX) and the stress for steel. The evolution of microstructure was studied as a function of temperatures, pass reductions, speeds, and times in rolling schedules by Sellars and Whiteman [10] during the plate rolling of low-carbon manganese steel. The constitutive equations were written in terms of the temperature during the deformation, strains, and strain rate for the various recrystallization and recovery processes. Davenport et al. [11] standardized the constitutive equations in terms of Z and included the flow stress behavior for steel during hot deformation. Shen [9,12] and Shen et al. [13] developed constitutive equations involving the Z and carefully studied the effect of DRX, MDRX, and SRX on the microstructure evolution during the forging of Waspaloy turbine discs. In the present work, a generalized form of empirical laws similar to those proposed by Shen [9] are taken as the basis and the development of the proposed microstructural algorithm incorporates appropriate modifications to predict the behavior of various superalloys including Alloy 718.

Computations

Anderson et al. [14] were some of the pioneers in numerically simulating the grain growth in materials during the early 1980s. Beynon and Sellars [15] developed an approach that can calculate rolling loads and torques with an accurate prediction of mean flow stress. Modeling the dynamic microstructural events is important for determining flow stress levels, and hence rolling loads. Lin et al. [16] treated the microstructure evolution in the context of dislocation densities using viscoplastic equations for C-Mn steel. Mirza et al. [17] incorporated microstructure predicting algorithms in an FE package to determine the microstructure in aluminum alloys. Similar attempts can be found using the commercial FE packages such as FORGE [18-20], ABAQUS [21], LARSTRAN/SHAPE [22], and DEFORM [23,24]. Goerdeler et al. [22] and Hirch et al. [25] developed simulation procedures that can predict the grain orientation or texture in addition to the usual grain size prediction during the multi-stand rolling of aluminum alloys. Davenport et al. [11] suggest the incorporation of constitutive equations into first-stage equations, describing the stress at a given strain as a function of Z, and second-stage equations, resulting in a continuous flow stress curve. Serajzadeh [26,27] discusses an approach involving the basic balance laws coupled with the microstructural behaviors. The current work employs the deformation variables calculated from the FE formulation discussed in the previous section and uses the formulation discussed in the next section to model the microstructure as a separate microstructure analysis package.

Formulations

Some of the published works take specific recrystallization processes into consideration. The effects of DRX and MRX are discussed by Zhou et al. [28] on wrought Alloy 718 in hot deformation, and the kinetics of DRX is predicted by Serajzadeh [29]. Semiatin et al. [30] divide the DRX into discontinuous DRX (DDRX) and continuous DRX (CDRX) for low stacking fault-energy materials such as nickel-base alloys. Karhausen et al. [31] developed a procedure in which the effective strain used in the calculations is assumed to be a function of the volume recrystallized during the rolling process in predicting the microstructure during a five-pass rolling of Cr-V Steel. Pauskar and Shivpuri [32] introduced an averaging procedure for various families of grains as the deformation proceeds in various passes during the rolling of TMS-80R steel. Thomas et al. [4] developed a microstructure model for forging of Alloy 718. The formulation presented in the current work is applied on multi-stand rolling of various nickel-base superalloys.

Microstructure algorithm

The presented algorithm is applied in the context of rolling processes that are modeled with flow formulations described in the 'FE formulation of multi-stand rolling' section. However, minor modifications can be applied to the procedure presented in this paper in developing a generic approach to include other FE formulations used for simulating the rolling process. In the proposed approach, the development of microstructure variables is predicted along a streamline from the flow formulation of the rolling process during a pass. Examples of such streamlines in a pass from the FE analysis are shown in Figure 2.

For the rolling problem characterized by flow formulation, all nodes on the free surface coincide with points on the flow streamlines, and each node in the whole mesh is essentially an integral part of a flow streamline. In the case of the steady-state rolling process

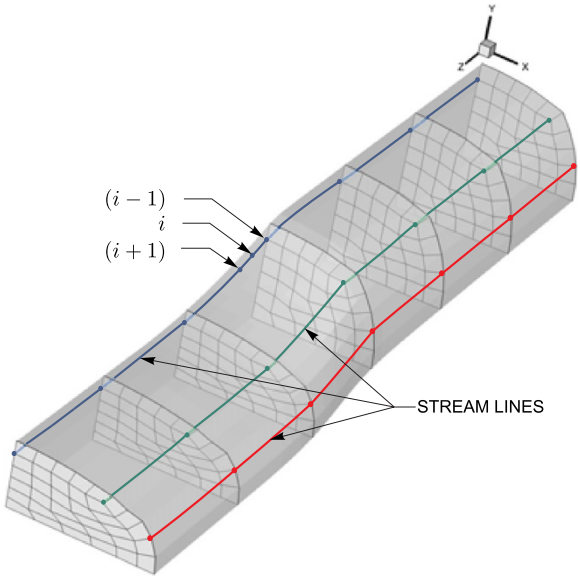

Figure 2 Typical streamlines from the 3D FE analysis (mesh from stand 3).

as described in this flow formulation, the deformation step is assumed to be characterized by the resident time at a particular node. The resident time is the time that elapses between a material particle's entry into the control volume and the time at its current location in space. Therefore, the microstructure evolution algorithm can be implemented in a dynamic fashion along the flow streamline. In addition, the microstructure is allowed to develop during interpass periods as well.

The FE code discussed earlier, predicts only the temperature distribution during the interpass by simulating a two-dimensional transient heat-transfer analysis. Therefore, the continuation of microstructure development is implemented along a hypothetical straight streamline whose nodes correspond to the points in time during the interpass. Typically, the points in time correspond to the locations in space since the rolled material moves during the interpass without undergoing any change in shape. The application of streamline outputs from commercial FE codes to calculate the evolution of material properties based on elementary rolling was implemented previously by Goerdeler et al. [22] in the context of aluminum alloys. Shen [9] employs an element-based approach in contrast to the presented node-based streamline approach for Waspaloy, in the context of forging analysis.

The proposed procedure considers two grain families: strained and recrystallized, at any given location in a streamline. A similar approach was developed by Thomas et al. [4]. Both the families of grains undergo recrystallization based on a deformation criterion discussed later. The schematic shown in Figure 3 shows that an initial uniform grain size, described by D_{st}, develops two grain families primarily characterized by the average volume recrystallized (F) and the average grain size (D).

The subscripts 'st' and 'rex' denote respectively the strained and recrystallized family of grains. These families undergo further recrystallization based on the achievement of certain critical parameters and develop into four subgroups. The strained family develops recrystallized grains characterized by (d_{strex}, X_{st}) that represent the instantaneous grain

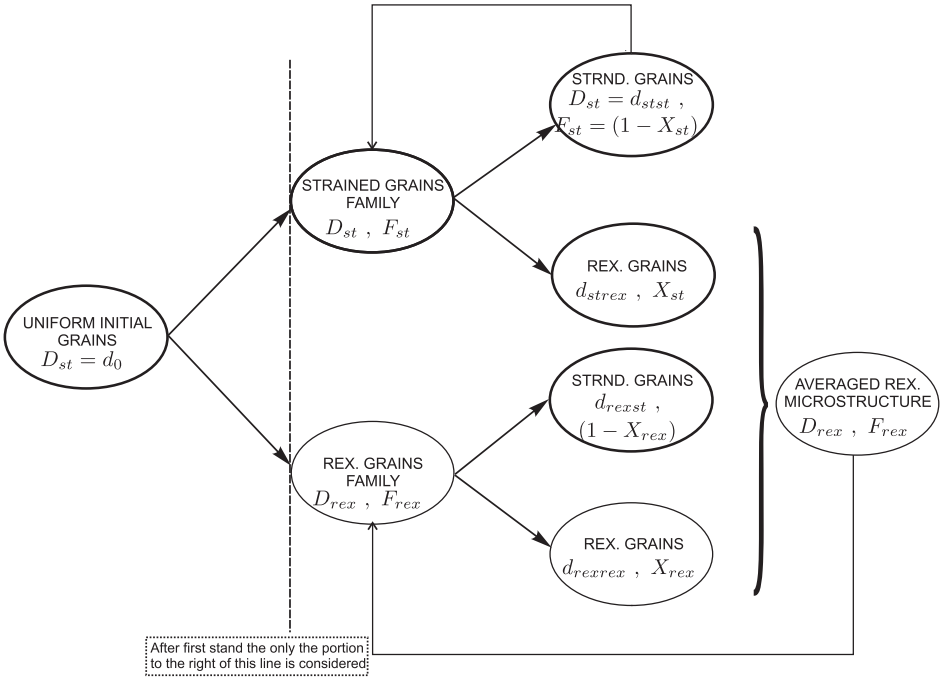

Figure 3 Microstructure families (a similar figure can be found in reference by Thomas et al. [4]).

size due to recrystallization laws and the recrystallization fraction, respectively. The non-recrystallized portion is the strained portion that is characterized by (d_{stst}, $(1-X_{\text{st}})$) which are functions of the recrystallized subgroup characteristics. A similar analogy is applicable to the recrystallized grain family subgroups and are characterized by (d_{rexrex}, X_{rex}) for the recrystallized portion and (d_{rexst}, $(1 - X_{\text{rex}})$) for the strained portions. These families are expected to evolve during the deformation in a pass and during interpass. Then, a weighted averaging algorithm is applied to calculate D_{rex} and F_{rex} prior to the achievement of critical deformation parameters during the next pass. D_{st} and F_{st} are calculated as follows:

$$D_{\text{st}} = D_{\text{st}} (1 - X_{\text{st}})^{\frac{1}{n\alpha}} \tag{5}$$

$$F_{\text{st}} = (1 - X_{\text{st}}) F_{\text{st}} \text{ or } = 1 - F_{\text{rex}}. \tag{6}$$

A detailed description of the microstructure evolution based on the deformation criterion can be explained with the schematic in Figure 4. The deformation during a pass is depicted with sawtooth lines at the bottom of the schematic. The figure is drawn for any arbitrary pair of stands with an interpass during continuous multi-stand rolling. The strain used for the microstructure calculation is given by Equation 7.

$$\bar{\varepsilon}_x^i = \bar{\varepsilon}^i + \nu(T)\bar{\varepsilon}_x^{(i-1)}, \tag{7}$$

where the subscript x can be st or rex to represent the strained and recrystallized families, $\bar{\varepsilon}^i$ is the instantaneous effective strain due to deformation, $\nu(T)$ is the temperature dependent factor used as a fraction for the previously stored strain $\bar{\varepsilon}_x^{(i-1)}$. The factor $\nu(T)$ varies between 0 and 1. The second term in Equation 7 denotes the retained strain from a previous pass. When this equivalent strain reaches a critical strain $\bar{\varepsilon}_c$, and if the effective strain rate $\dot{\bar{\varepsilon}}$ reaches a material dependent value greater than equal to $\dot{\bar{\varepsilon}}_c$, DRX is initiated.

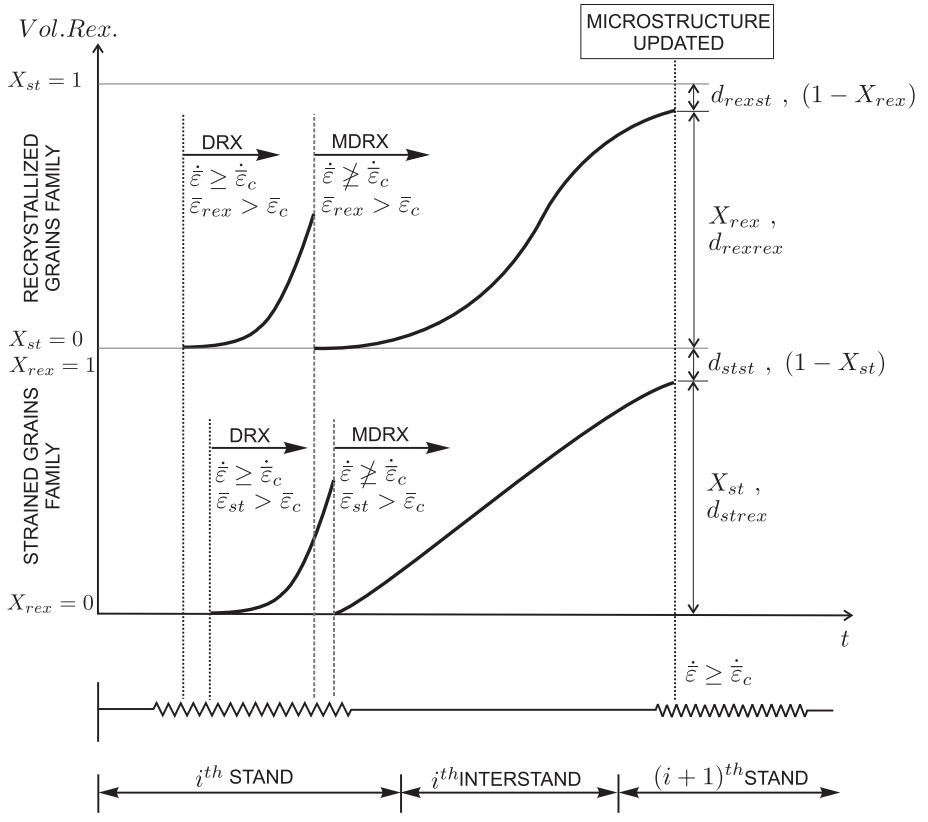

Figure 4 Microstructure evolution of different families.

Consider a single streamline shown in the Figure 5, extracted from Figure 2. Based on Figure 5, the strain rate is calculated as,

$$\dot{\bar{\varepsilon}} = \frac{\delta\bar{\varepsilon}}{\delta t} = \frac{\bar{\varepsilon}^i - \bar{\varepsilon}^{i-1}}{t^i - t^{i-1}}. \tag{8}$$

MDRX follows DRX and does not require the strain rate to be greater than $\dot{\bar{\varepsilon}}_c$. However, the need for critical strain to be achieved still holds. MDRX assumes that the recrystallization initiates from the beginning; even though, some of the grains may be partially recrystallized due to DRX. The initial grain size used for MDRX calculations are the original initial grain sizes used in calculating the DRX grain size. That is, DRX is considered

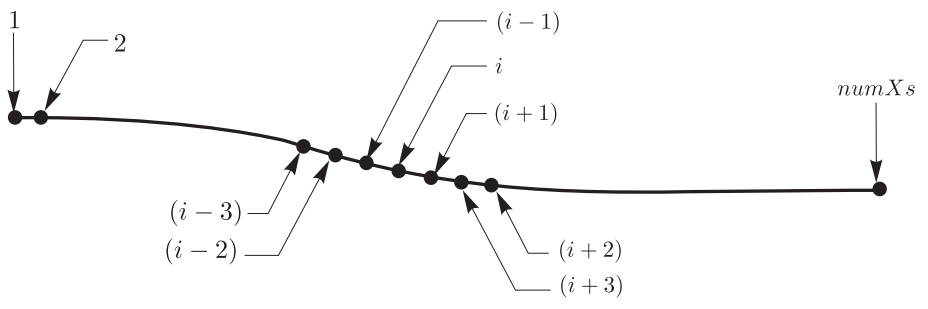

Figure 5 Nodes on a streamline.

only as a recrystallization initiation process and the contribution to the microstructure is primarily due to MDRX. When the recrystallization fraction reaches a set value greater than 90%, the grains at the location corresponding to the applicable node are assumed to be fully recrystallized and static grain growth is initiated until further deformation changes the microstructure evolution process. In this work, the nodes in the FE mesh are considered to follow the streamline, and the nodal deformation variables are used in calculating the microstructure variables.

Implementation

Empirical laws describing the various processes mentioned above establish the relationships between grain size and process parameters such as tool and workpiece geometry, temperature, deformation speed, and amount of deformation through regression analysis of experimental data as developed by Huang et al. [8] and Shen [9]. Recrystallization is a continuously evolving process, and an instantaneous application of the empirical laws may not capture the continuous nature of the process under consideration. In addition, the actual deformation is not an isothermal process. The approach described in this section calculates the evolution based on time integration detailed in the following.

Dynamic recrystallization

The rate of DRX increases with an increase in temperature and strain and decreases with an increase in the strain rate. For a particular location in a streamline, this can be observed from the expression for fraction recrystallized expressed as,

$$X = 1 - \exp\left(-\ln(2)\left[\frac{\bar{\varepsilon}}{\bar{\varepsilon}_{0.5}}\right]^a\right), \tag{9}$$

where $\bar{\varepsilon}_{0.5}$ refers to the strain at which the grains are 50% recrystallized. In other words, $\bar{\varepsilon}_{0.5}$ refers to the strain at which $X = 0.5$ and is expressed as follows:

$$\bar{\varepsilon}_{0.5} = d\,(d_o)^c(\dot{\bar{\varepsilon}})^{d_1}\,\exp\left(d_2\frac{Q_h}{R\bar{T}}\right). \tag{10}$$

In order to capture the continuous evolution of the fraction recrystallized, a time integration is necessary that incorporates the increment in strain in each increment of time. Accordingly, the recrystallization fraction for DRX is a function of the equivalent strain named as the virtual strain in this work. That is,

$$X = f(\bar{\varepsilon}_v). \tag{11}$$

Rewriting Equation 9 in line with Equation 11,

$$X = 1 - \exp\left[-\ln(2)\left(\frac{\bar{\varepsilon}_v}{\bar{\varepsilon}_{0.5}}\right)^a\right]$$

we find that the virtual strain is given by,

$$\bar{\varepsilon}_v = \bar{\varepsilon}_{0.5}\left(\frac{\ln(1-X)}{-\ln(2)}\right)^{\frac{1}{a}}. \tag{12}$$

During rolling, the material undergoes deformation continuously under the rolls and the strain continues to increase and so does the recrystallization fraction. In general, the recrystallization fraction for DRX during rolling is the sum of the recrystallization

fraction from previous deformation and an incremental recrystallization fraction from the current deformation. That is,

$$X^i = X^{i-1} + \delta X^{i-1}. \tag{13}$$

In terms of virtual strain, the right-hand side of Equation 13 can be expressed as,

$$X^i = 1 - \exp\left[-\ln(2)\left(\frac{\bar{\varepsilon}_\nu^{i-1} + \delta\bar{\varepsilon}^{i-1}}{\bar{\varepsilon}_{0.5}^{i-1}}\right)^a\right]. \tag{14}$$

From Figure 5, initially $i = 1, X^0 = 0$, and therefore,

$$\begin{aligned}\bar{\varepsilon}_\nu^0 &= \bar{\varepsilon}_{0.5}^0\left[\frac{\ln(1-X^0)}{-\ln(2)}\right]^{\frac{1}{a}}\\ &= 0.\end{aligned}$$

This algorithm is incorporated into an interactive package entitled GRANARY (the microstructure prediction package developed for the current work) for DRX based on the achievement of certain critical strain. The critical strain is expressed as a fraction of the peak strain. A peak strain is a material and process-dependent variable. The peak strain, critical strain, and the strain corresponding to 50% recrystallization for any location are given by,

$$\overline{\varepsilon}_c = n_{\text{dynctop}}\,\overline{\varepsilon}_p, \tag{15}$$

$$\overline{\varepsilon}_p = f\, d_o^g \dot{\bar{\varepsilon}}^{h_1}\, \exp\left(h_2\frac{Q_h}{R\overline{T}}\right), \tag{16}$$

and

$$\overline{\varepsilon}_{0.5}^{(i)} = d\,(d_o)^c(\dot{\bar{\varepsilon}})^{d_l}\, \exp\left(d_2\frac{Q_h}{R\overline{T}}\right). \tag{17}$$

Equations 14 through 17 are evaluated by substituting the strain rate calculated using Equation 8 and average temperature calculated using the following expression,

$$\overline{T}^i = \frac{T^i + T^{i+1}}{2}.$$

The grain size expression developed by empirical methods gives only the grain size at the steady state, that is when the recrystallization is 100% complete. However, the grain size also evolves continuously and the instantaneous grain size need to be incorporated in the recrystallization fraction. Equation 18 is the commonly found expression for the steady-state grain size due to recrystallization. Equation 19 is the instantaneous recrystallized grain size as a function of the fraction recrystallized. The third expression (given by Equation 20) denotes the grain size of the strained grains in the current family of grains.

$$d_{\text{drx}}^{(ss)} = p(\dot{\bar{\varepsilon}})^{q_1}\, \exp\left(q_2\frac{Q_d}{R\overline{T}}\right), \tag{18}$$

$$d_{\text{drx}}^{(i)} = d_{\text{drx}}^{(ss)}\left(X^{(i)}\right)^{n_{\text{xdrx}}}, \tag{19}$$

and

$$d_{\text{str}}^{(i)} = d_0\left(1 - X^{(i)}\right)^{n_{\text{xdrxst}}}. \tag{20}$$

In these expressions, the following parameters,

$$n_{\text{xrex}},\ n_{\text{xrexst}},\ Q_h,\ Q_d,\ n,\ Q_p,\ a*,\ b*,\ c*,$$
$$d1*,\ p*,\ q1*,\ f*,\ g*,\ h1*,\ h2*,\ d2*,\ q2*,$$

are pertinent to the specific material and are described in the nomenclature. For those parameters with the symbol $*$, they are further defined specifically

$$\begin{aligned}&\text{for sub-solvus } \left(\overline{T} < 1,010^{\circ}\text{C}\right),\\ &\text{for solvus } \left(\overline{T} = 1,010^{\circ}\text{C}\right),\\ &\text{for super-solvus } \left(\overline{T} > 1,010^{\circ}\text{C}\right).\end{aligned}$$

As a first step to describing similar laws for Alloy 718, the empirical laws that describe the behavior of Waspaloy found in the literature by Shen [9] were incorporated into the microstructure algorithm as one of the many models that may be utilized by the user.

Metadynamic recrystallization

When DRX is not 100% complete, further recrystallization occurs without the addition of any strain which is characterized as MDRX. During MDRX, the recrystallization fraction is primarily a function of the time (t) and a time constant ($t_{0.5}$) at which the recrystallization is 50% complete. The general expression is similar to Equation 9, and the curve is a similar sigmoidal curve, except that the independent strain variable $\overline{\varepsilon}$ is replaced by time variable t indicating the fact that MDRX evolves with time. The time at which 50% recrystallization occurs can be expressed in general by the following equation:

$$t_{0.5} = b\, d_o^c\, \overline{\varepsilon}^f\, \dot{\overline{\varepsilon}}^{d_1}\, \exp\left(d_2\, \frac{Q_h}{R\overline{T}}\right). \tag{21}$$

In the present work, the average strain rate during deformation has been incorporated to calculate this variable. To capture the continuous evolution of MDRX, an approach similar to that developed in the previous section is applied which includes a virtual time similar to the virtual strain shown in Equation 14. The following equations for the grain sizes due to MDRX are similar to Equations 18, 19, and 20 for calculating the grain sizes due to DRX,

$$\begin{aligned}d_{\text{mdrx}}^{ss} &= p\, d_0^s\, \overline{\varepsilon}^r\, \dot{\overline{\varepsilon}}^{q_1}\, \exp\left(q_2 \frac{Q_d}{R\overline{T}}\right),\\ d_{\text{mdrx}}^{(i)} &= d_{\text{mdrx}}^{(ss)} \left(X^{(i)}\right)^{n_{\text{xmdrx}}},\end{aligned}$$

and

$$d_{\text{str}}^{(i)} = (1 - \left(X^{(i)}\right)^{n_{\text{xmdrxst}}}.$$

Similar empirical parameters in the aforementioned expressions can be found from the literature by Huang et al. [8], Shen [9], Yeom et al. [33] for various superalloy materials.

Static grain growth

When the MDRX process is 100% complete, and the material does not undergo any additional strain, annealing occurs. Any extended hold at elevated temperatures causes the grains to grow statically. There are quadratic and cubic laws that describe the static grain growth. A general expression that describes the static grain growth is expressed by Equation 22,

$$d_{\text{ggr}} = \left[d_{\text{ini}}^{n_{\text{ggr}}} + t_{\text{ggr}} \delta t \exp\left(\frac{-Q_{\text{ggr}}}{R\overline{T}}\right)\right]^{\frac{1}{n_{\text{ggr}}}}, \tag{22}$$

where the parameters n_{ggr}, t_{ggr}, and Q_{ggr} can be found from literature. The grain growth typically occurs during the long interpasses and during hold times at the end of the rolling process.

Results and discussion

The presented microstructure algorithm can predict the microstructure evolution during the multi-stand rolling of nickel-base superalloys such as Waspaloy and Alloy 718. The algorithm was applied on three nickel-base superalloys: i) Waspaloy, ii) Alloy 718, and iii) a proprietary alloy. In this paper, for the verification of the developed algorithm, only the results from Alloy 718 are presented based on a proprietary rolling pass schedule that was used to carry out the FE analysis of rolling. This paper presents predicted results in comparison with the actual observed microstructure for a four-stand rolling followed by air cooling and for a 16-stand rolling followed by a combination of air and water cooling. The mesh considered for the rolling and microstructure analysis was developed with five core divisions and one outer division (see Figure 6a). The details of the core and outer divisions are given in the 'FE formulation of multi-stand rolling' section in line with Figure 1. Figure 6a shows some locations with symbols ●, ◆, ▼, ■, and ▲ chosen to study the history of microstructure evolution over many stands. These locations characterize center, mid radius, sub surface, and surface locations chosen to permit a comparison of predicted microstructure results with the experimental observations.

Based on a separate mesh sensitivity study, it was determined that the chosen mesh, that is, five core and one outer division, gives accurate enough results when compared with the measured temperature and shape at intermediate and final stands. It is to be noted, that the calculations are carried out at each node in a cross section and each node constitutes a point on a streamline.

Since the deformation variables are extracted to the nodes from the integration points, nodal variables are chosen to predict the microstructure. In the current work, the parameters used for Waspaloy and Alloy 718 are similar to those found in the literatures by Shen [9] and Huang et al. [8], respectively, for DRX. Parameters similar to those used in

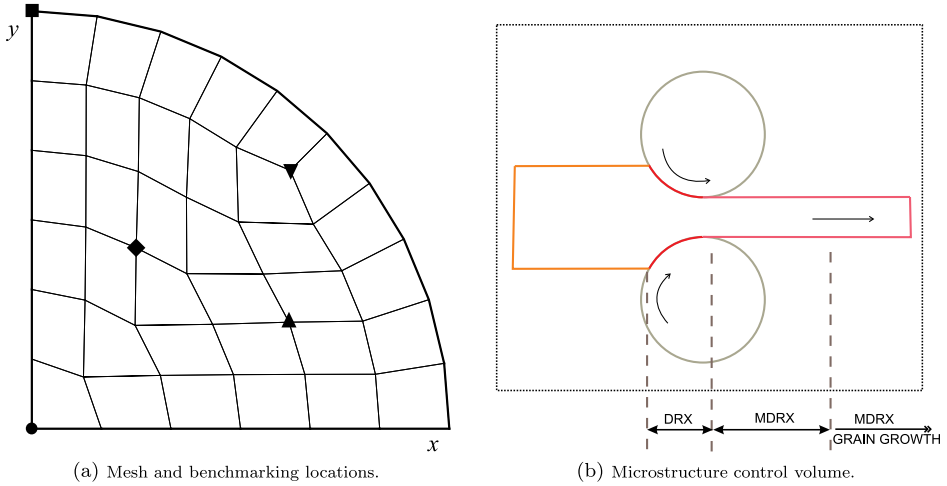

(a) Mesh and benchmarking locations. (b) Microstructure control volume.

Figure 6 Mesh considered (a) and the schematic control volume in a pass (b).

the current work for the MDRX process and grain size calculation during MDRX can be found in literature by Huang et al. [8] and by Yeom et al. [33]. The static grain growth was calculated based on cubic laws similar to those found in the reference by Shen [9]. An initial uniform grain size of 90 μm (ASTM rating 4) is used as input to the analysis.

Cooling

Two scenarios are considered. In the first case that corresponds to four-stand rolling, at the end of rolling, the bars are assumed to be air cooled. At high strain rates, quench/cooling time becomes a critical parameter for MDRX. In addition, the micrographs to compare the predicted results were captured at the end of 4th stand with 5 s of air cooling. In the case of a second scenario that corresponds to the 16-stand rolling process, the cooling is primarily due to water. In the analysis, at the end of the 16th stand, a combination of air and water quenching is applied. Firstly, an air cooling for 2 s captures the time for transferring the billet, and an additional 2 s captures the evolution during immersion water quenching. This type of combined cooling is considered to mimic the process for which the micrograph results are available.

As a brief review of the discussion made in the previous section, Figure 6 gives a larger picture of the microstructure evolution process. That is, DRX process under the rolls as deformation continues, MDRX in the region close to the rolls and a continuation of the MDRX and a static grain growth during the interpass or cooling depending on the achievement of 100% recrystallization.

Four-stand analysis with air cooling at the end of the 4th stand

The temperature and equivalent strain histories at the chosen locations are shown in Figures 7 and 8, respectively. From these figures, it can be observed that the strains are low in the initial two stands, specifically very low during the 2nd pass with a maximum value of 0.25. In Figure 8, the independent axis is not to scale. That is, the interpass times are much larger compared to the pass times, and hence, the figure was created with actual strains and not-to-scale times.

Sixteen-stand analysis with air and water cooling at the end of the 16th stand

The temperature and equivalent strain history at the chosen locations (see Figure 6a) are shown in Figures 9 and 10, respectively. In Figure 10, the plot was created with actual strains and not-to-scale times since the interpass times are much larger compared to the pass times. From these figures, it can be observed that the instantaneous equivalent strains reach values as high as 1.45 during the 13th stand. Similarly, due to severe deformations imposed during the later stands, the temperatures also experience a significant increase.

Streamline results

Figures illustrating the effectiveness of the presented microstructure algorithm were developed with normalized variables such as temperature, strain, and other microstructure variables over time for the recrystallized and strained families of grains on streamlines passing through the considered locations. For simplicity, only the discussion of the observations are presented here in the context of the four-stand analysis, and the reader is encouraged to see reference [34] for details.

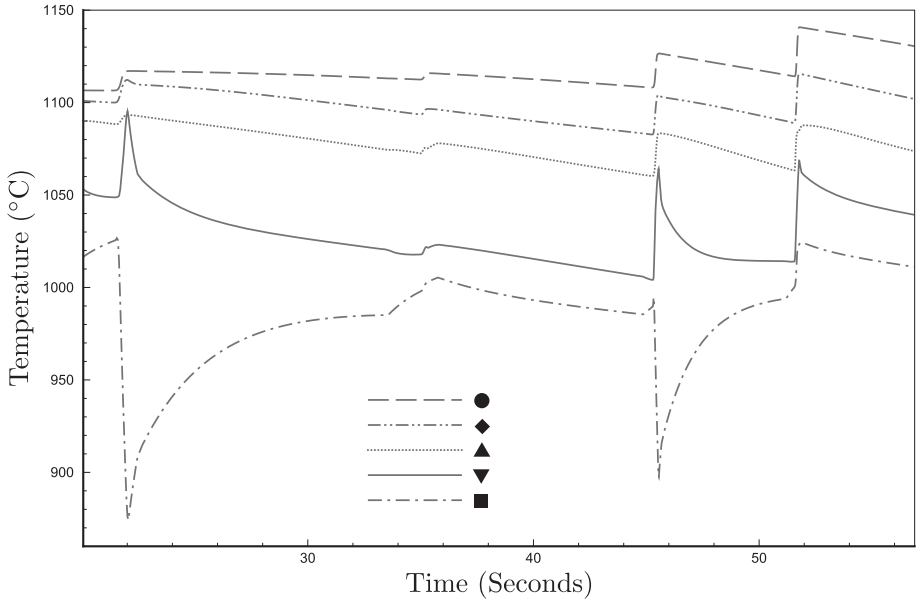

Figure 7 Temperature history on various streamlines (four-stand analysis). (At time ranges 20 to 23 s, 34 to 36 s, 45 to 46 s, and 51 to 52 s, the bar is under the rolls in stands 1, 2, 3, and 4, respectively, undergoing deformation).

At the central location represented by ●, recrystallization initiates with DRX and continues with MDRX as soon as the addition of the strain stops and progresses until the recrystallization is complete during the interpass. The strains are reset to zero for the strained family, and the grains start to grow statically during the interpass. Prior to achieving the strain rate and critical strain condition in the second pass, the

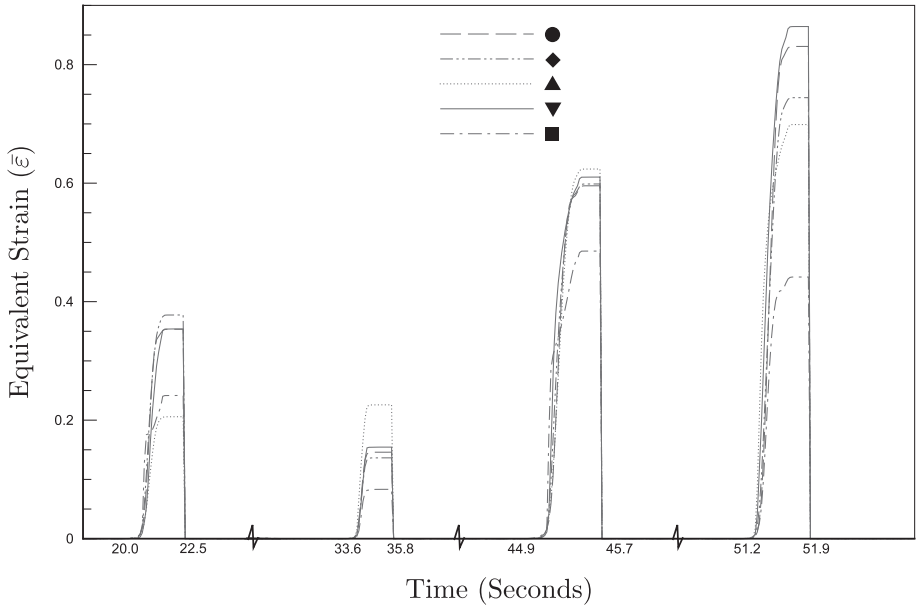

Figure 8 Strain history on various streamlines (four-stand analysis).

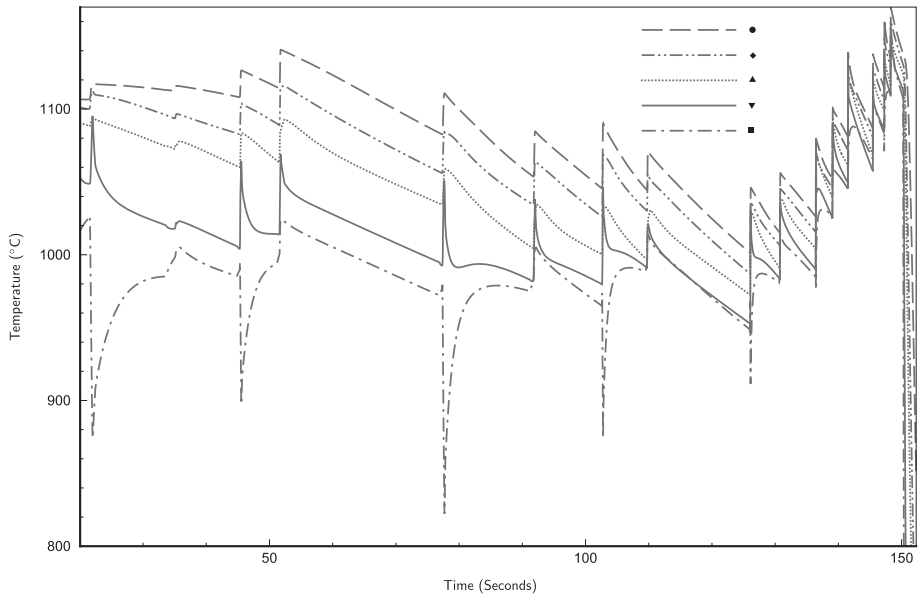

Figure 9 Temperature history on various streamlines (16-stand analysis).

microstructure averaging algorithm updates the microstructure, and F_{st} is set to zero if all the grains at this location are fully recrystallized.

During the deformation in the 2nd stand, the recrystallized family undergoes recrystallization and the MDRX does not recrystallize the REX family of grains fully. However, due to the high strains and temperatures in stand 3, the MDRX completes and a similar phenomenon is observed in stand 4 as well. Therefore, at this location, at the end of 4th stand, only the recrystallized family exists and the grain size is approximately 70 μm.

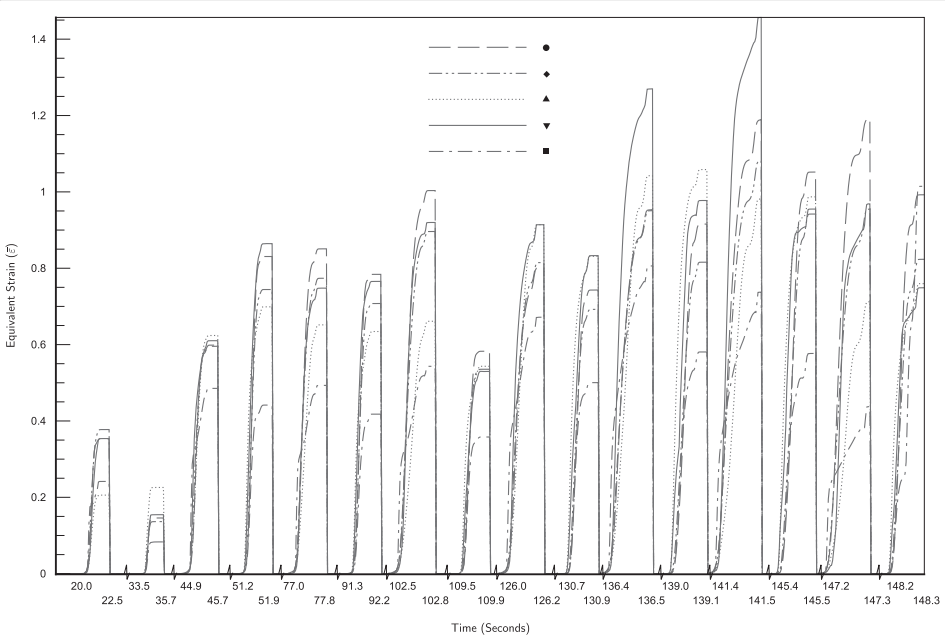

Figure 10 Strain history on various streamlines (16-stand analysis).

Similar characteristics are observed at the interior locations represented by ◆ and ▼; however, a rapid grain growth is observed at the location represented by ▼. For the location indicated by the symbol ▲, the strained family of grains vanish only at the end of 2nd stand. On the other hand, it takes four stands for the surface location indicated by the symbol ■ to recrystallize completely.

If the air cooling is not considered at the end of 4th stand but an interpass is assumed to continue the analysis, an interesting phenomenon is observed in the case of the subsurface location (indicated by ▼) where an insignificant portion of strained grain family experienced full recrystallization during the 9th interpass. However, this does not contribute much to the global microstructure characteristics. At the surface location represented by ■, contains both strained and recrystallized grain families till the 6th stand and then the strained grain family vanishes.

More details on the microstructure evolution for all the locations studied can be found in the literature by the first author [34].

Final observations for the four-stand analysis

A contour plot of the recrystallized fraction (F_{rex}) at the beginning of the deformation during the 4th stand and the recrystallized fraction (X_{rex}) at the end of the air cooling analysis after the 4th stand are depicted in Figure 11a,b, respectively. F_{rex} is calculated based on the averaging algorithm proposed in the 'Formulations' subsection. It can be observed that there are very few portions in the cross section near the surface that are not fully recrystallized.

An observation on the grain sizes due to Figure 12a,b indicates that the region near the core experienced a significant grain growth due to the high temperatures while the surface regions show smaller grains. Figure 13 indicates the observed microstructure at various locations and the grain sizes at those locations. It is clear that the grains show signs of complete recrystallization at all locations and groups of recrystallized families as seen in Figure 13c. Also, at the center (Figure 13a) the grains are largest and smaller at the midradius location (Figure 13b) while they are smallest at the surface (Figure 13c).

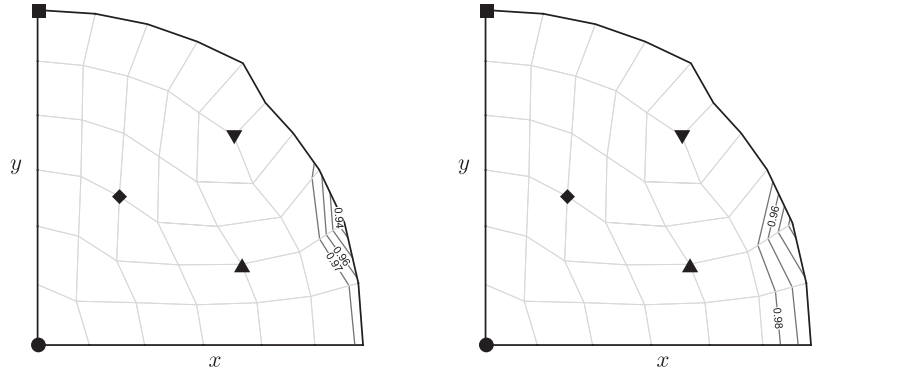

(a) F_{rex} at the beginning of Stand-4. (b) Fraction Rec. X_{rex} at the end of cooling.

Figure 11 Recrystallization fractions (×100%) during (a) the 4th stand and after (b) air cooling after the 4th stand.

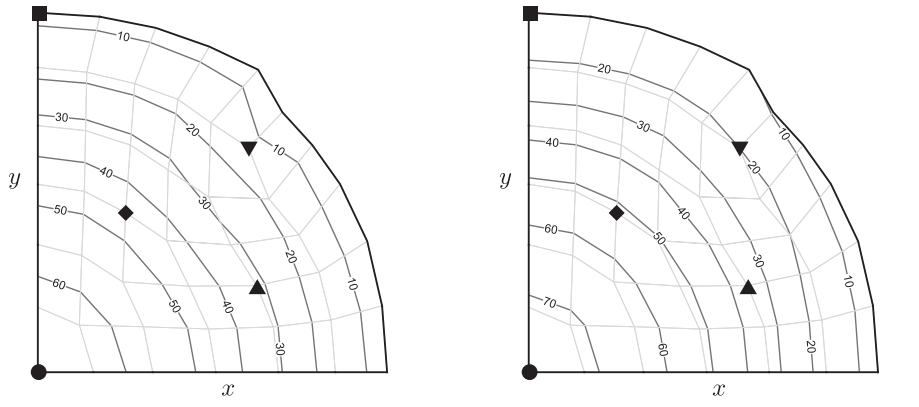

(a) Initial REX. grain size (D_{rex}). (b) Rec.REX grain size (d_{rexrex}).

Figure 12 REX family grain size (μm) after (a,b) air cooling at the end of the 4th stand.

Final observations for the 16-stand analysis

This section describes the results at the end of the 16th stand if the rolling continued without any cooling at the end of 4th stand but with interpass conditions.

A contour plot of the recrystallized grain sizes characterized by the variables D_{rex} and d_{rexrex} are shown in Figure 14. The grain size distribution is almost uniform around 20 μm (see Figure 14a) for the D_{rex} which characterizes the overall grain size distribution while the recrystallized grains (represented by d_{rexrex} in Figure 14b) show slightly larger grains close to the center, since the center does not cool quickly. The actual microstructure observed at the end of cooling after 16-stand rolling of the considered material is shown in Figure 15. The calculated microstructure results are in good agreement with the observed microstructure.

Discussion

The predicted microstructure from the presented approach is in good agreement with the observed microstructure for the four-stand analysis and for the 16-stand analysis.

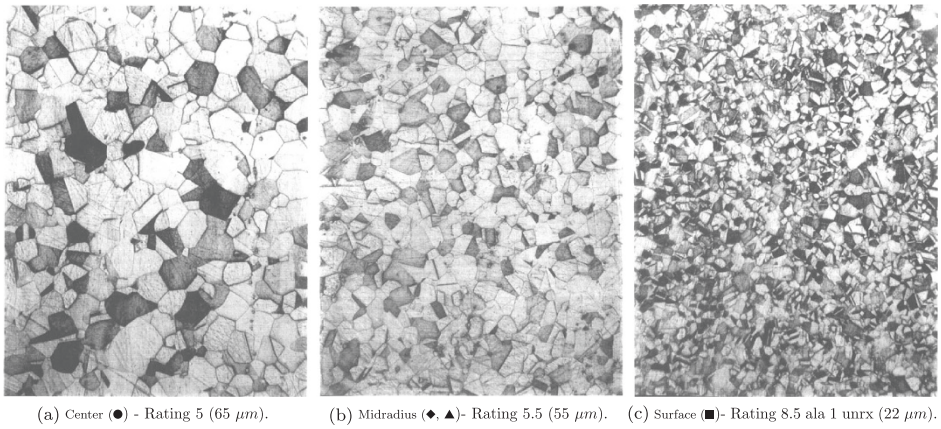

(a) Center (●) - Rating 5 (65 μm). (b) Midradius (◆, ▲)- Rating 5.5 (55 μm). (c) Surface (■)- Rating 8.5 ala 1 unrx (22 μm).

Figure 13 Various locations (a-c) and observed microstructure at the end of the 4th stand after 5 s of air cooling.

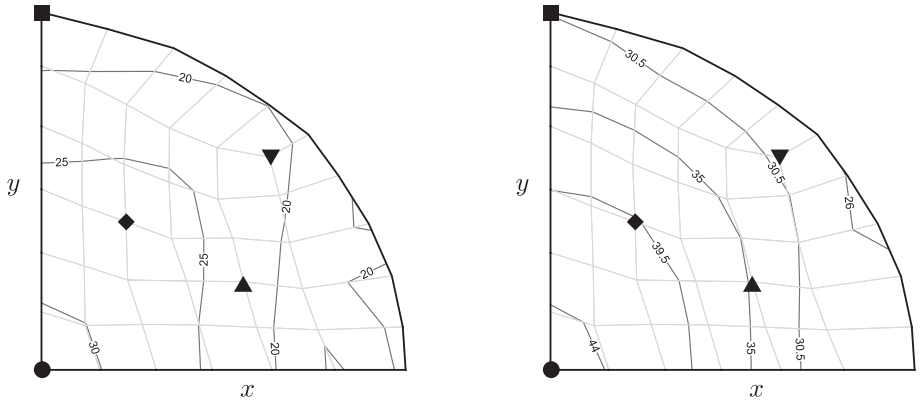

(a) Initial Rec. Grain Size (D_{rex}). (b) Rec. Grain Size (d_{rexrex}).

Figure 14 Grain sizes (μm) at the end (a,b) of cooling after the 16th stand.

When microstructural processes such as DRX occur, the increases in strain and temperature favors dynamic softening. Grain size is a function of the deformation variables such as temperature, strain, and strain rate. Temperature enhances dynamic softening and, as observed during the later stands where a significant increase in temperature occurs, the grain sizes tend to increase. Strain influences the microstructure significantly as observed by other authors [4,35,36]. An increased rate in MDRX after deformation at high strain rates as a result of adiabatic heating is explained by Brand et al. [3]. The streamline figures confirm this conclusion. The fraction recrystallized due to DRX increases due to increase in the addition of strain, and the accumulated strain at the end of deformation influences the MDRX since DRX does not completely recrystallize the grains in any case for Alloy 718 material.

The variation of grain size is correlative to the behavior of work hardening and dynamic softening existing in Alloy 718 during hot deformation. When the temperature increases, dynamic softening occurs and the grain size increases. When the strain rate increases, work hardening occurs and the grain size decreases. Increasing the holding

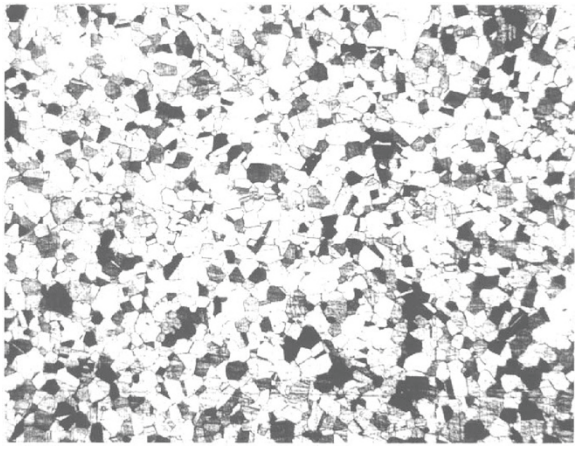

Figure 15 Uniform microstructure at any location at the end of the 16th stand. (ASTM 8 or 22 μm uniform) (courtesy: ATI Allvac).

time increases the volume fraction recrystallized. Long holding times after deformation allows complete recrystallization of microstructure. This is witnessed during the interpasses, where the MDRX is a significant contributor.

Conclusions

The prediction of microstructure by employing appropriate empirical models available in the literature requires a rigorous approach that captures the evolution of the microstructure. The current work encompassed the development of such a comprehensive procedure and its validation in the context of three superalloys, with results presented specifically for Alloy 718 in this paper. The predicted numerical results are in good agreement with the observed microstructure for a four-stand and a 16-stand multi-pass rolling involving different cooling conditions at the end of the rolling process by incorporating suitable empirical models found in literature for various microstructural processes.

In summary, the presented procedure incorporates the approach by which a total recrystallization fraction is calculated by taking into account the residual strain and also incorporates a total recrystallized fraction that incorporates fractions of previously recrystallized grain families. The developed procedure assumes that the grain matrix does not contain excessive δ phase. However, δ phase disappears at temperatures above 1,000°C, close to the solvus temperature of ≈1,010°C. In addition, the observed temperatures are mostly above the solvus region, and the averaging procedure is considered applicable in predicting the microstructure dominated by γ matrix. The predicted microstructure results are in agreement with the observed microstructures within 1 ASTM number of the grain size. In the current work, the microstructure is considered isotropic and equiaxed. In the future, this algorithm will be tested for other superalloy materials and stands beyond 16 in designing a generic forming process.

Nomenclature

J^*	Potential Energy Functional
Ω	Domain
Γ_t	Traction-specified boundary
$\bar{T}_i$	Components of the traction vector
u_i	Velocity component
$\dot{\varepsilon}_{ij}$	Components of the strain rate tensor
σ'_{ij}	Components of the deviatoric stress tensor
δa	Small increment or variation in a quantity a
a_{ii}	Summation implied over the index i implied on any quantity a
$\boldsymbol{I}$	Second-order identity tensor
p	Hydrostatic pressure
a^T	Transpose of the quantity a
μ	Viscosity
$\boldsymbol{u}$	Velocity vector
$\boldsymbol{f}$	Force vector
$\boldsymbol{p}$	Pressure
$\mathbf{K}_D$	Global stiffness matrix for velocity
$\mathbf{Q}$	Global stiffness matrix for pressure
γ	Penalty parameter

θ	Temperature variable
κ	Boltzmann's constant
ϵ	Emissivity
$\bar{\theta}$	Defined temperature
q_r	Heat flux due to radiation
q_h	Heat flux due to convection
DRX	Dynamic recrystallization
MDRX	Metadynamic recrystallization
u_i	ith component of velocity
D	Average grain size
F	Average volume recrystallized
R	Universal gas constant
$\bar{\varepsilon}_c$	Critical strain
F_{rex}	Fraction of recrystallized grains due to averaging
D_{rex}	Grain size of recrystallized grains due to averaging
D_{st}	Grain size of the strained grains due to averaging
F_{st}	Fraction of strained grains due to averaging
d_{strex}	Instantaneous recrystallized grain size evaluated using the equations for the strained grain family
d_{stst}	Instantaneous strained grain size evaluated using the equations for the strained grain family
d_{rexrex}	Instantaneous recrystallized grain size evaluated using the equations for the recrystallized grain family
d_{rexst}	Instantaneous strained grain size evaluated using the equations for the recrystallized grain family
n_α	Exponent for calculating the strained grain size
ν	Fraction to find the retained strain
$\bar{\varepsilon}_{0.5}$	Strain at which the grains are 50% recrystallized during DRX
a	Temperature-specific DRX or MDRX parameter to evaluate X and $\bar{\varepsilon}_{0.5}$ for DRX and $t_{0.5}$ for MDRX
b	MDRX parameter to evaluate X and $t_{0.5}$
c	Temperature-specific DRX or MDRX parameter to evaluate X and $\bar{\varepsilon}_{0.5}$ for DRX and $t_{0.5}$ for MDRX
d	Temperature-specific DRX parameter to evaluate X and $\bar{\varepsilon}_{0.5}$
d_1	Temperature-specific DRX or MDRX parameter to evaluate X and $\bar{\varepsilon}_{0.5}$ for DRX and $t_{0.5}$ for MDRX
d_2	Temperature-specific DRX por MDRX parameter to evaluate X and $\bar{\varepsilon}_{0.5}$ for DRX and $t_{0.5}$ for MDRX
Q_h	Activation energy for DRX and MDRX in evaluating respectively the $\bar{\varepsilon}_{0.5}$ and $t_{0.5}$
Q_d	Activation energy for DRX and MDRX in evaluating the steady state grain size
$\bar{\varepsilon}_p$	Peak strain
f	Temperature-specific parameter to evaluate $\bar{\varepsilon}_p$ during DRX and a parameter to evaluate X and $t_{0.5}$ during MDRX
g	Temperature-specific DRX parameter to evaluate $\bar{\varepsilon}_p$
h_1	Temperature-specific DRX parameter to evaluate $\bar{\varepsilon}_p$

h_2	Temperature-specific DRX parameter to evaluate $\bar{\varepsilon}_p$
n_{dynctop}	Fraction to calculate the critical strain $\bar{\varepsilon}_c$
d_0	Initial grain size used in evaluating the microstructure variables
$\bar{\varepsilon}_v$	Virtual strain
d_a^{ss}	Steady state grain size when recrystallization is 100% for any grain family represented by a
n_{xdrx}	Exponent to calculate the instantaneous grain size due to DRX
n_{xdrxst}	Exponent to calculate the instantaneous strained grain size due to DRX
$t_{0.5}$	Time required to achieve 50% recrystallization during MDRX
t_v	Virtual time
p	MDRX parameter to evaluate the steady-state grain size
s	MDRX parameter to evaluate the steady-state grain size
r	MDRX parameter to evaluate the steady-state grain size
q_1	MDRX parameter to evaluate the steady-state grain size
q_2	MDRX parameter to evaluate the steady-state grain size
n_{xmdrx}	Exponent to calculate the instantaneous grain size due to MDRX
n_{xmdrxst}	Exponent to calculate the instantaneous strained grain size due to MDRX
d_{ggr}	Grain size during static grain growth
n_{ggr}	Exponent denoting the type of grain growth law (quadratic or cubic)
t_{ggr}	Grain growth parameter which is material specific
Q_{ggr}	Activation energy for grain growth
$\overline{T}$	Average temperature used in microstructure calculations

Competing interests
The authors declare that they have no competing interests.

Authors' contributions
KS did all the formulations and prepared the article. HPC discussed the simulation results and corrected the article. Both authors read and approved the final manuscript.

Acknowledgements
Financial support for this research work is provided by ATI Allvac, Monroe, NC. The authors express gratitude towards Drs. Minisandram and Thomas from ATI Allvac for their valuable inputs on Alloy 718 and multi-stand rolling simulation.

Author details
[1]Stress Engineering Services, Inc., 3314 Richland Ave, 70002 Metairie, LA, USA. [2]Department of Mechanical Engineering and Engineering Science, University of North Carolina at Charlotte, 9201 University City Blvd, 28223 Charlotte, NC, USA.

Received: 21 July 2014 Accepted: 7 November 2014
Published online: 25 November 2014

References

1. Minisandram RS, Thompson EG, Forbes Jones RM, Stedje-Larsen R (2001) Numerical simulation of a multi-stand rolling mill. In: Mori K (ed). Proceedings of the 7th international conference on numerical methods in industrial forming processes - NUMIFORM 2001, Toyohashi, Japan, 18–21 June 2001. Swets & Zeitlinger B.V., Lisse
2. Subramanian K, Minisandram RS, Cherukuri HP (2007) Mesh re-zoning in multi-stand rolling. In: César de Sá JMA (ed). Proceedings of the 9th international conference on numerical methods in industrial forming processes - NUMIFORM 2007, Porto, Portugal, 17–21 June 2007. American Institute of Physics (API), College Park
3. Brand AJ, Karhausen K, Kopp R (1996) Microstructural simulation of nickel based inconel 718 in production of turbine discs. Mater Sci Tech 12(11):963–969
4. Thomas JP, Bauchet E, Dumont C, Montheillet F (2004) EBSD Investigation and modelling of the microstructural evolutions of superalloy 718 during hot deformation. In: Green KA (ed). Proceedings of Superalloys 2004. The Minerals, Metals & Materials Society (TMS), Warrendale. pp 959–968
5. Zienkiewicz O (1984) Flow formulation for numerical solution of forming processes. In: Numerical analysis of forming processes. Wiley, New York. pp 1–69
6. Humphreys FJ, Hatherly M (2004) Recrystallization and related annealing phenomena. Elsevier, Oxford
7. Sellars CM (1978) Recrystallization of metals during hot deformation. Philos T Roy Soc A 288(1350):147–158
8. Huang D, Wu WT, Lambert D, Semiatin SL (2001) Computer simulation of microstructure evolution during hot forging of waspaloy and nickel alloy 718. In: Srinivasan R, Semiatin SL, Beaudoin A, Fox S, Jin Z (eds). Proceedings of

symposium: microstructure modeling and prediction during thermomechanical processing, Indianapolis, November 4–8 2001. TMS, Warrendale. pp 137–147
9. Shen G (1994) Modeling microstructural development in the forging of waspaloy turbine engine disks. Dissertation, Ohio State University
10. Sellars CM, Whiteman JA (1979) Recrystallization and grain growth in hot rolling. Met Sci 13:187–194
11. Davenport SB, Silk NJ, Sparks CN, Sellars CM (2000) Development of constitutive equations for modelling of hot rolling. Mat Sci Tech 16(5):539–546
12. Shen G (2005) Microstructure modeling in superalloy forging. In: Altan T (ed). Cold and hot forging: fundamentals. ASM International, Novelty. pp 247–255
13. Shen G, Semiatin SL, Shivpuri R (1995) Modeling microstructural development during the forging of waspaloy. Metall Mater Trans A 26(7):1795–1803
14. Anderson MP, Srolovitz DJ, Grest GS, Sahni PS (1983) Computer simulation of grain growth – I. Kinetics. Acta Metall 32(5):783–791
15. Beynon JH, Sellars CM (1992) Modeling microstructure and its effects during multipass hot rolling. ISIJ Intl 32(3):359–367
16. Lin J, Liu Y, Farrugia DCJ, Zhou M (2005) Development of dislocation-based unified material model for simulating microstructure evolution in multipass hot rolling. Phil Mag 85(18):1967–1987
17. Mirza MS, Sellars CM, Karhausen K, Evans P (2001) Multiphase rolling of aluminium alloys: finite element simulation and microstructural evolution. Mat Sci Tech 17(7):874–879
18. Kusiak J, Kuziak R, Wajda W, Kowalski B (1999) Finite-element modeling of forging of nickel based superalloys. In: Kanagy DL (ed). Proceedings of 41st Mechanical Working and Steel Processing Conference, Baltimore, Maryland, October 24–27 1999. Iron and Steel Society, London, vol. XXXVII. pp 683–688
19. Dandre CA, Walsh CA, Evans RW, Reed RC, Roberts SM (2000) Microstructural evolution of Inconel 718 during ingot breakdown: process modelling and validation. Mat Sci Tech 16(1):14–26
20. Duan X, Sheppard T (2001) Prediction of temperature evolution by FEM during multi-pass hot flat rolling of aluminum alloys. Model Sim Mater Sci Engng 9(6):525–538
21. Mukhopadhyay A, Howard IC, Sellars CM (2004) Development and validation of a finite element model for hot rolling using ABAQUS/STANDARD. Mat Sci Tech 20(9):1123–1133
22. Goerdeler M, Crumbach M, Gottstein G, Neumann L, Luce R, Kopp R, Allen CM, Winden Mvd, Karhausen K (2002) Integral modeling of texture evolution in multiple pass hot rolling in aluminium alloys. Mat Sci Forum 396–402:379–386
23. Phaniraj MD, Behera BB, Lahiri AK (2006) Thermo-mechanical modeling of two phase rolling and microstructural evolution in the hot strip mill Part II. - Microstructure evolution. Mat Proc Tech 178(1–3):388–394
24. Zhao D, Cheng C, Anbajagane R, Dong H, Suarez FS (1997) Three-dimensional computer simulation of alloy 718: Ingot breakdown by cogging. In: Loria EA (ed). Proceedings of the 4th International Symposium on Superalloys 718, 625, 706 and Various Derivatives, Pittsburgh, Pennsylvania, June, 15–18 1997. The Minerals, Metals & Materials Society (TMS), Warrendale. pp 163–172
25. Hirch J, Karhausen K, Kopp R (1994) Microstructural simulation during hot rolling of Al-Mg Alloys. In: Proceedings of the 4th International Conference on Aluminium Alloys, Atlanta, Georgia, Georgia Institute of Technology, School of Materials Science & Engineering, Atlanta. pp 476–483
26. Serajzadeh S (2003) Prediction of microstructural changes during hot rod rolling. Int J Mach Tools Manf 43(14):1487–1495
27. Serajzadeh S (2005) Thermomechanical modeling of hot slab rolling. Mat Sci Tech 21(1):93–102
28. Zhou LX, Baker TN (1995) Effects of dynamic and metadynamic recrystallization on microstructures of wrought IN-718 due to hot deformation. Mat Sci Engng A 196(1–2):89–95
29. Serajzadeh S (2004) Prediction of dynamic recrystallization kinetics during hot rolling. Model Sim Mat Sci Engng 12(6):1185–1200
30. Semiatin SL, Weaver DS, Fagin PN, Glavicic MG, Goetz RL, Frey ND, Kramb RC, Antony MM (2004) Deformation and recrystallization behavior during hot working of a coarse-grain, nickel-base superalloy ingot material. Metall Mater Trans A 35(2):679–693
31. Karhausen K, Kopp R, de Souza MM (1991) Numerical simulation method for designing thermomechanical treatments, illustrated by bar rolling. Scandinavian J Metall 20(6):351–363
32. Pauskar P, Shivpuri R (1999) Microstructure and mechanics interaction in the modeling of hot rolling of rods. CIRP Annals Manuf Tech 48(1):101–104
33. Yeom JT, Lee CS, Kima JH, Park NK (2007) Finite-element analysis of microstructure evolution in the cogging of an alloy 718 ingot. Mat Sci Eng A 449–451:722–726
34. Subramanian K (2009) Microstructure evolution during multi-stand rolling of nickel-base superalloy. Dissertation, University of North Carolina at Charlotte
35. Guest RP, Tin S (2005) The dynamic and metadynamic recrystallisation of the in 718. In: Loria EA (ed). Proceedings of the 6th international symposium on superalloys 718, 625, 706 and various derivatives, Pittsburgh PA, October 2–5 2005. The Minerals, Metals & Materials Society (TMS), Warrendale
36. Zhang JM, Gao ZY, Zhuang JY, Zhong ZY (1999) Mathematical modeling of the hot deformation behaviour of superalloy in718. Metall Mater Trans A 30(10):2701–2712

doi:10.1186/s40192-014-0027-3
Cite this article as: Subramanian and Cherukuri: **Prediction of microstructure evolution during multi-stand shape rolling of nickel-base superalloys.** *Integrating Materials and Manufacturing Innovation* 2014 **3**:27.